Electronic Supporting Information for

Dual-cubic-cage based lanthanide sulfate-carboxylpyrazolate frameworks with highly hydrolytic stability and remarkable proton conduction

Liang He,[a,b] Jayanta Kumar Nath,[a] Erxia Chen,[a] Hengdong Lai,[a] Shanlin Huang[a] and Qipu Lin*[,a]

[a]*State Key Laboratory of Structural Chemistry Fujian Institute of Research on the Structure of Matter, Chinese Academy of Sciences, Fuzhou, Fujian 350002, China*

[b]*College of Materials Science and Engineering Fujian Normal University, Fuzhou, Fujian 350007, China*

*Corresponding Author: Email: linqipu@fjirsm.ac.cn

Table of Contents

Section S1: General Methods

Chemicals: All chemical reagents were obtained from commercial supplies without further purification.

Instrumentation: Elemental analysis (EA) was carried out on a Vario EL-Cube. Powder X-ray diffraction (PXRD) patterns of the samples were recorded by a Rigaku Dmax 2500 X-ray diffractometer with Cu *K*α radiation (λ = 1.54056 Å). Metal contents were measured by an Ultima2 (Horbiba Jobin Yvon) inductively coupled plasma optical emission spectrometer (ICP-OES). Thermal analysis was carried out on a Netzsch STA449C thermal analyzer at a temperature range of 25 to 800 °C under air atmosphere with a heating rate of 10 °C min^{-1}. Gas sorption measurements were performed on a Micromeritics ASAP 2020 surface area and pore size analyzer. Fourier-transform infrared (FT-IR) spectra were recorded using a Nicolet iS10 spectrophotometer in 3750~450 cm^{-1} region.

Section S2: Synthetic Procedures of Ln-SCP

(1) Synthesis of Eu-SCP

Eu_2O_3 (0.25 mmol, 0.088 g), H_3PDC (0.5 mmol, 0.086 g), $ZnSO_4·7H_2O$ (0.25 mmol, 0.072 g and water (15 mL) were mixed in a 23 mL teflon-lined stainless steel container and stirred for 30 min, then heated to 150 °C for 60 h. After cooling to room temperature at 5 °C min^{-1}, single crystals were obtained after washing with water (ca. 35% yield based on H_3PDC). EA data: C 11.76%; H 2.43%; N 5.36%; S 4.50. ICP data: Eu 39.40%; Zn 0.94%.

(2) Synthesis of Gd-SCP

Gd_2O_3 (0.25 mmol, 0.091 g), H_3PDC (0.5 mmol, 0.086 g), $ZnSO_4·7H_2O$ (0.25 mmol, 0.072 g and water (15 mL) were mixed in a 23 mL teflon-lined stainless steel container and stirred for 30 min, then heated to 150 °C for 60 h. After cooling to room temperature at 5 °C min^{-1}, single crystals were obtained after washing with water (ca. 35% yield based on H_3PDC). EA data: C 12.71%; H 2.37%; N 5.89%; S 4.67. ICP data: Gd 37.46%; Zn 1.44%.

(3) Synthesis of Dy-SCP

Dy_2O_3 (0.25 mmol, 0.093 g), H_3PDC (0.5 mmol, 0.086 g), $ZnSO_4·7H_2O$ (0.25 mmol, 0.072 g and water (15 mL) were mixed in a 23 mL teflon-lined stainless steel container and stirred for 30 min, then heated to 150 °C for 60 h. After cooling to room temperature at 5 °C min^{-1}, single crystals were obtained after washing with water (ca. 35% yield based on H_3PDC). EA data: C 10.26%; H 2.35%; N 4.98%; S 5.13. ICP data: Dy 40.56%; Zn 1.53%.

(4) Synthesis of Ho-SCP

Ho_2O_3 (0.25 mmol, 0.094 g), H_3PDC (0.5 mmol, 0.086 g), $ZnSO_4·7H_2O$ (0.25mmol, 0.072g and water (15 mL) were mixed in a 23 mL teflon-lined stainless steel container and stirred for 30 min, then heated to 150 °C for 60 h. After cooling to room temperature at 5 °C min^{-1}, single crystals were obtained after washing with water (ca. 30% yield based on H_3PDC). EA data: C 9.13%; H 2.24%; N 4.23%; S 5.54. ICP data: Ho 38.21%; Zn 1.00%.

Section S3: Crystallographic Data

Table S1 Crystallographic data of Ln-SCP

Compound Reference	Eu-SCP	Gd-SCP	Dy-SCP	Ho-SCP
Chemical Formula	$(C_{60}H_{96}Eu_{20}N_{24}O_{138}S_{12})\cdot$ [+guests]	$(C_{60}H_{96}Gd_{20}N_{24}O_{138}S_{12})\cdot$ [+guests]	$(C_{60}H_{96}Dy_{20}N_{24}O_{138}S_{12})\cdot$ [+guests]	$(C_{60}H_{96}Ho_{20}N_{24}O_{138}S_{12})\cdot$ [+guests]
Formula Mass	7052.59	7162.04	7270.54	7320.77
Crystal System	Cubic	Cubic	Cubic	Cubic
a/Å	17.7222(4)	17.7222(4)	17.5393(3)	17.5393(3)
b/Å	17.7222(4)	17.7222(4)	17.5393(3)	17.5393(3)
c/Å	17.7222(4)	17.7222(4)	17.5393(3)	17.5393(3)
α/°	90	90	90	90
β/°	90	90	90	90
γ/°	90	90	90	90
Unit-Cell Volume/ Å^3	5566.1(4)	5566.1(4)	5395.6(3)	5395.6(3)
Temperature/K	293(2)	293(2)	293(2)	293(2)
Space Group	*Pm*-3	*Pm*-3	*Pm*-3	*Pm*-3
No. of Formula Units Per Unit-Cell, *Z*	1	1	1	1
No. of Reflections Measured	36501	36309	34574	41961
No. of Independent Reflections	1817	1805	2270	2239
R_{int}	0.0537	0.0831	0.0423	0.0252
Final R_1 Values ($I > 2\sigma(I)$)	0.0349	0.0416	0.0217	0.0219
Final $wR(F^2)$ Values ($I > 2\sigma(I)$)	0.0794	0.0934	0.0559	0.0639
Final R_1 Values (all data)	0.0349	0.0416	0.0225	0.0220
Final $wR(F^2)$ Values (all data)	0.0794	0.0934	0.0565	0.0643
Goodness of Fit on F^2	1.064	1.042	1.046	1.016
CCDC Number	1880636	1880637	1880638	1880639

Section S4: Structural Pictures

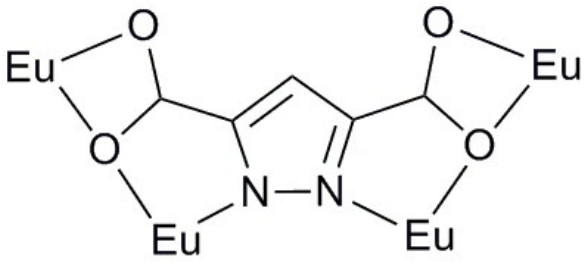

Fig. S1 PDC^{3-} ligand and its coordination mode in Eu-SCP.

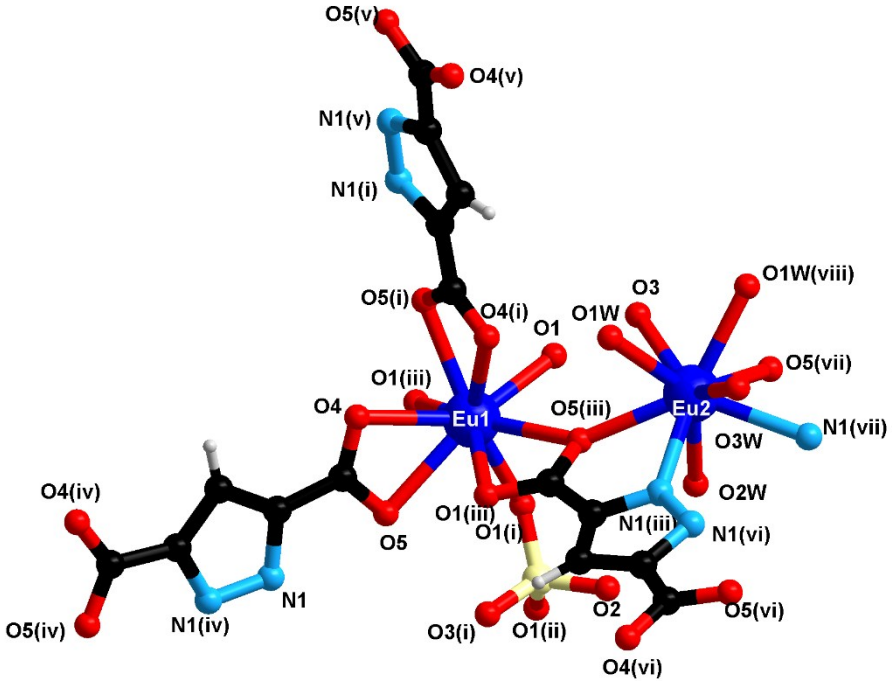

Fig. S2 Coordination environments of Eu^{3+} ions in Eu-SCP (symmetry codes: (i) y, z, x; (ii) –y, z, x; (iii) z, x, y; (iv) x, 1-y, z; (v) 1-y, z, x; (vi) z, x, 1-y; (vii) z, -x, y; viii) x, -y, z).

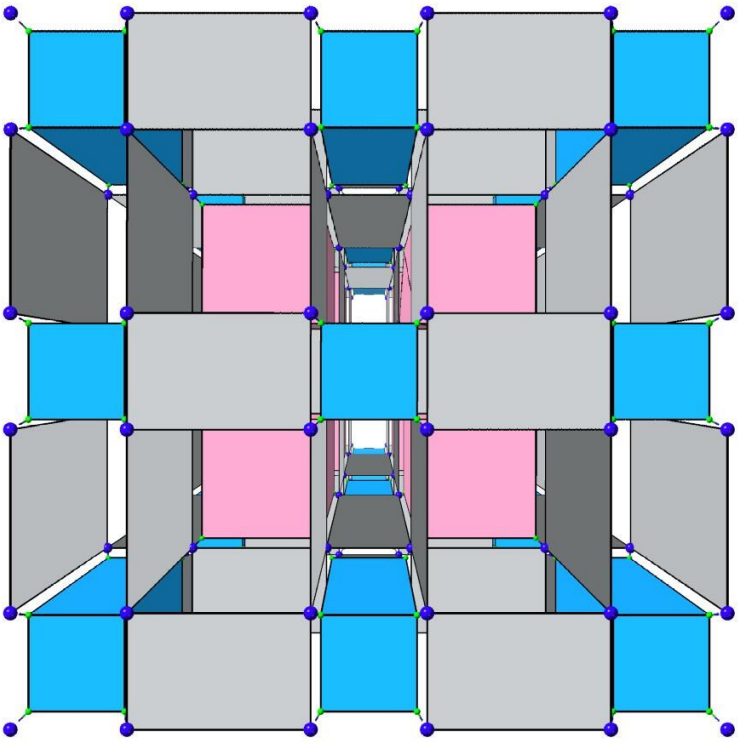

Fig. S3 Rectangular tile-based structure of Eu-SCP containing two kinds of cubic cages denoted by pink and blue cubes.

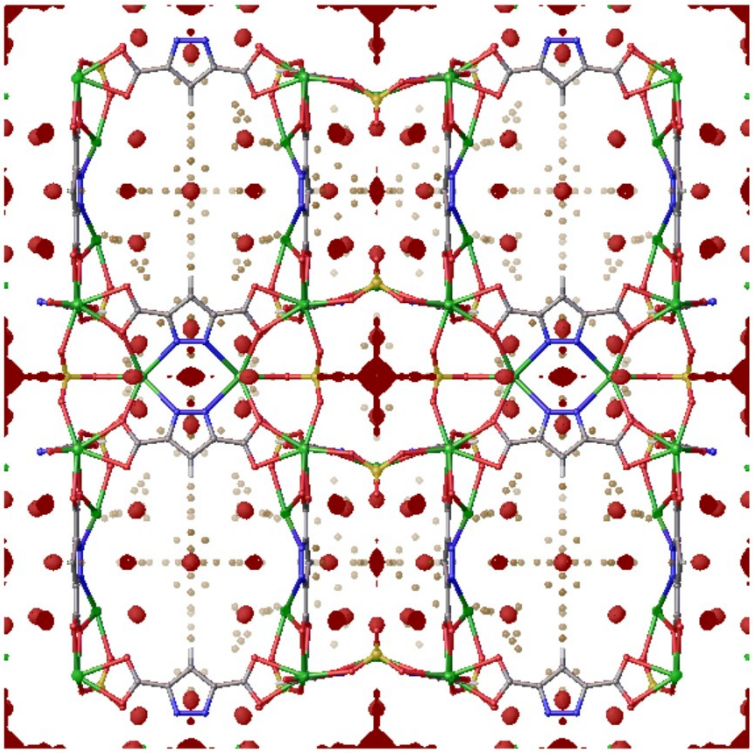

Fig. S4 Electron density map in the cavity region of Eu-SCP produced by X-ray crystallography.

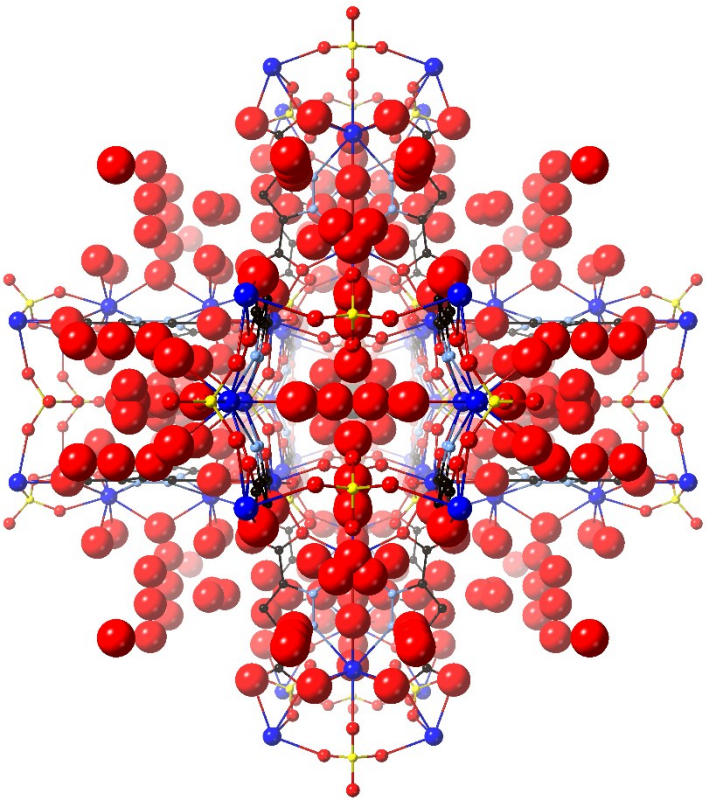

Fig. S5 Proton-transfer pathways of Eu-SCP constructed by host sulfate, guest complex, coordinated and lattice water arrayed orderly.

Section S5: Photography

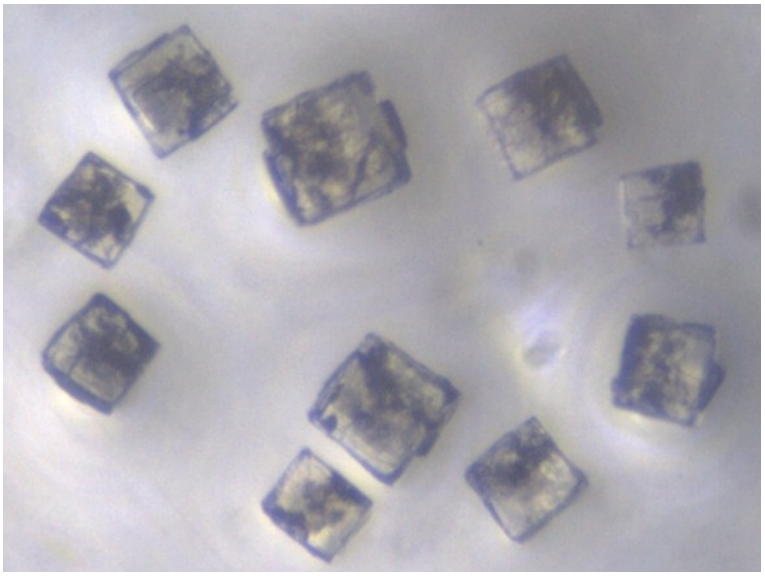

Fig. S6 Microscopic image of Eu-SCP sample.

Section S6: Fourier-Transform Infrared (FT-IR) Spectroscopy

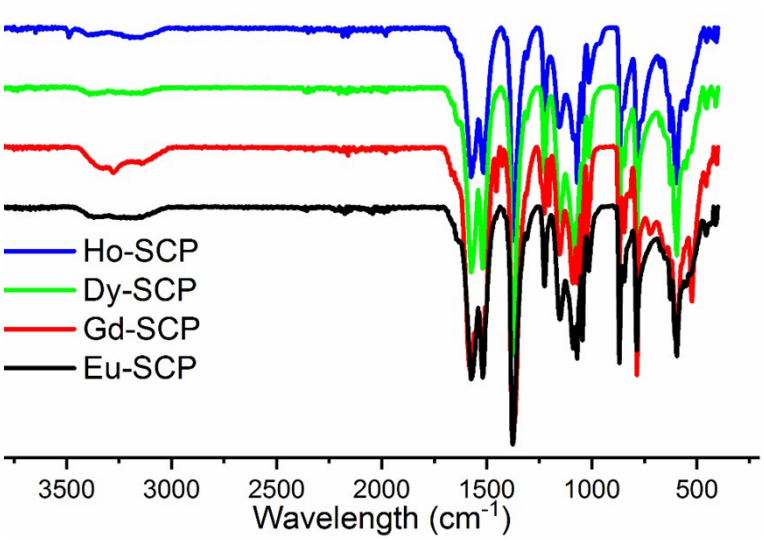

Fig. S7 FT-IR spectra of Eu-SCP, Gd-SCP, Dy-SCP and Ho-SCP.

Section S7: Powder X-ray Diffraction (PXRD)

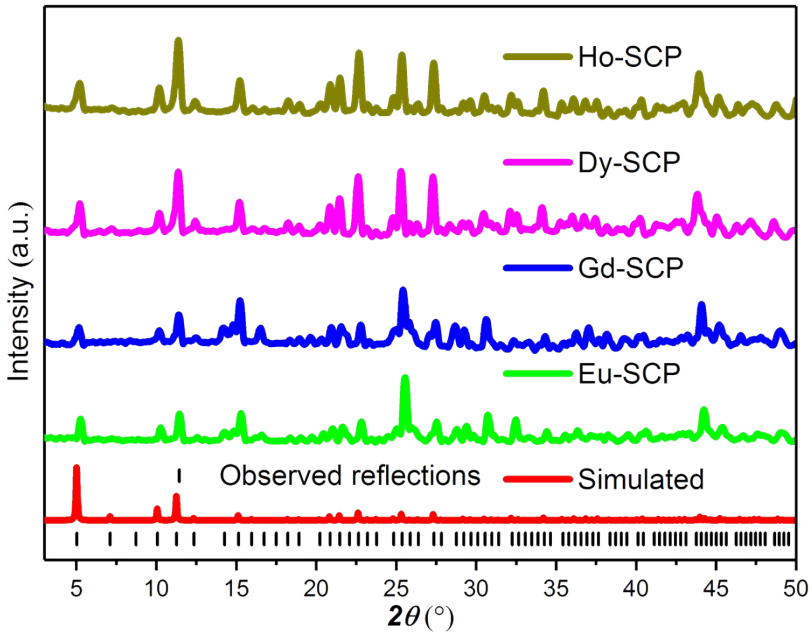

Fig. S8 PXRD patterns of Eu-SCP, Gd-SCP, Dy-SCP and Ho-SCP.

Section S8: Stability Analysis

(a) Thermal Gravimetric Analysis (TGA)

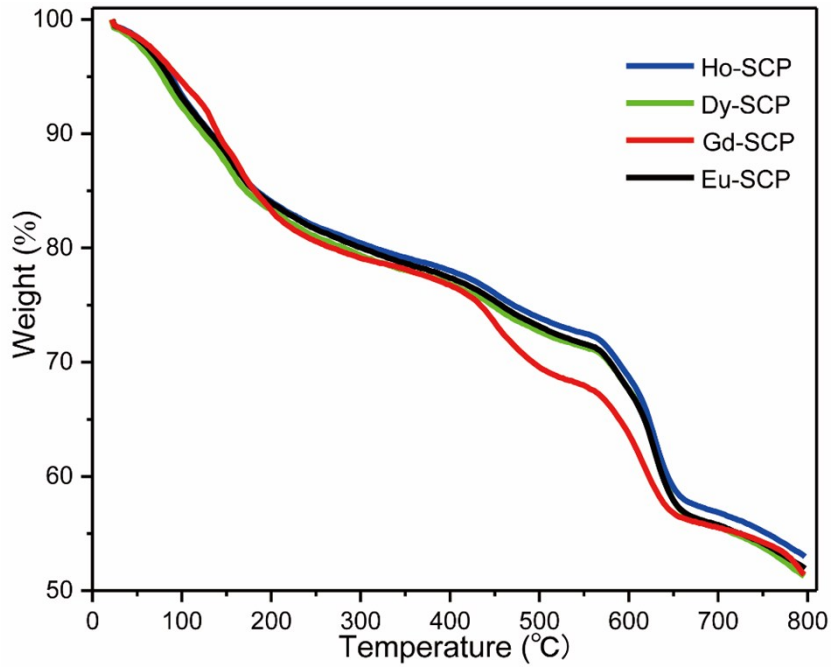

Fig. S9 TGA curves of Eu-SCP, Gd-SCP, Dy-SCP and Ho-SCP in the air.

(b) Thermal PXRD

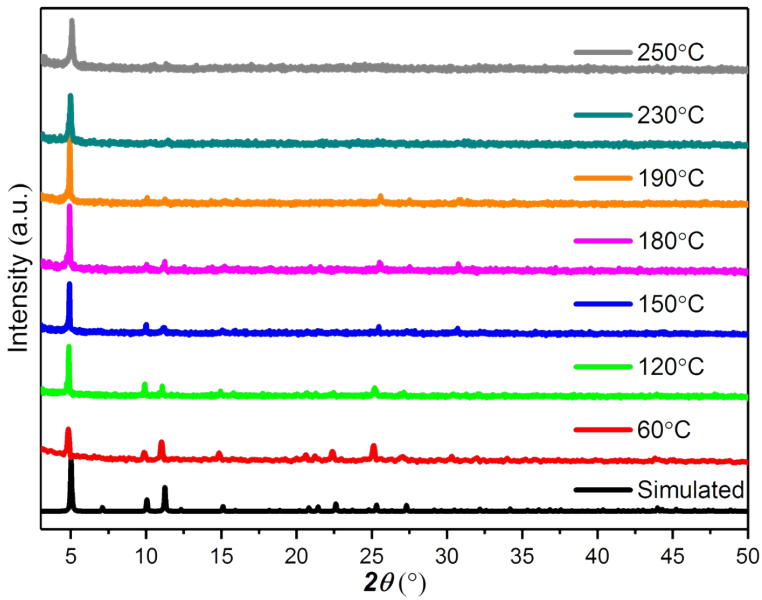

Fig. S10 Thermal PXRD patterns of Eu-SCP, indicating that the sample could be stable upto 250 °C.

(c) Chemical Stability Analysis

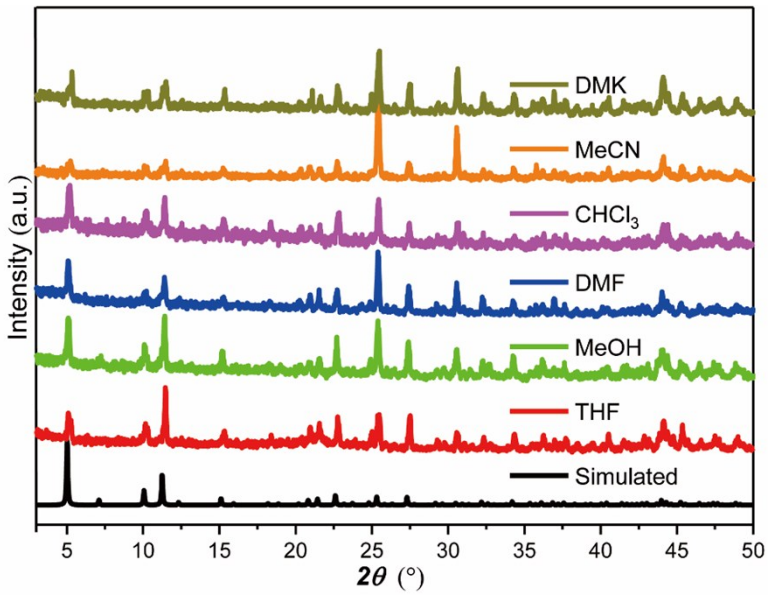

Fig. S11 PXRD patterns of Eu-SCP in different organic solvents for 20 h.

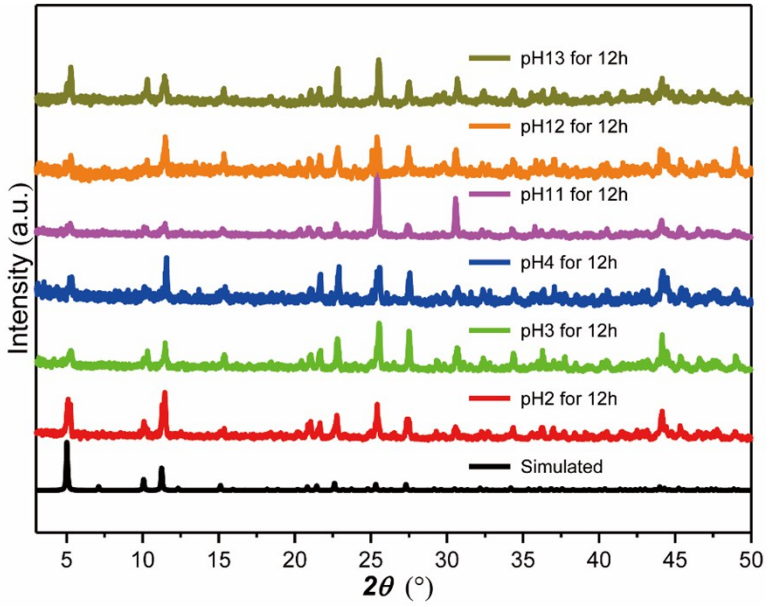

Fig. S12 PXRD patterns of Eu-SCP in different pH water for 12 h.

Section S9: Gas-Sorption Measurements

The samples were activated by soaking in CH_3OH three days and CH_3OH was renewed two times every day before testing.

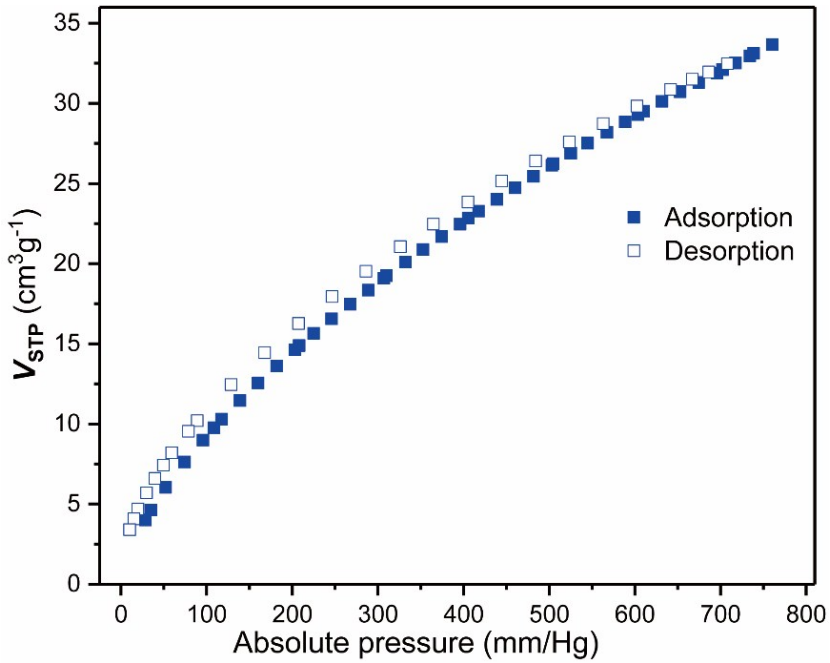

Fig. S13 CO_2 adsorption-desorption isotherms of Eu-SCP at 298 K.

Section S10: Ultraviolet-Visible (UV-Vis) Spectroscopy

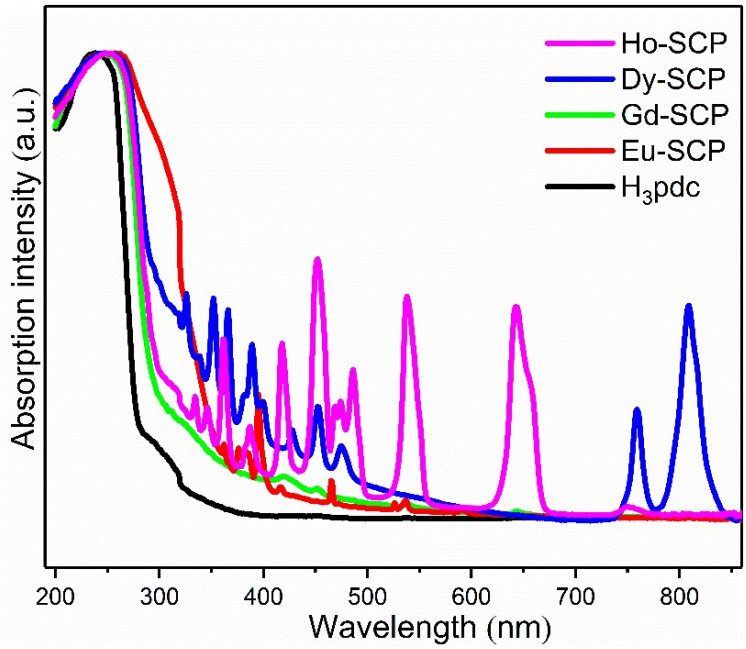

Fig. S14 UV-Vis diffuse-reflectance spectra of Eu-SCP, Gd-SCP, Dy-SCP, Ho-SCP and H_3PDC.

Section S11: Photoluminescence

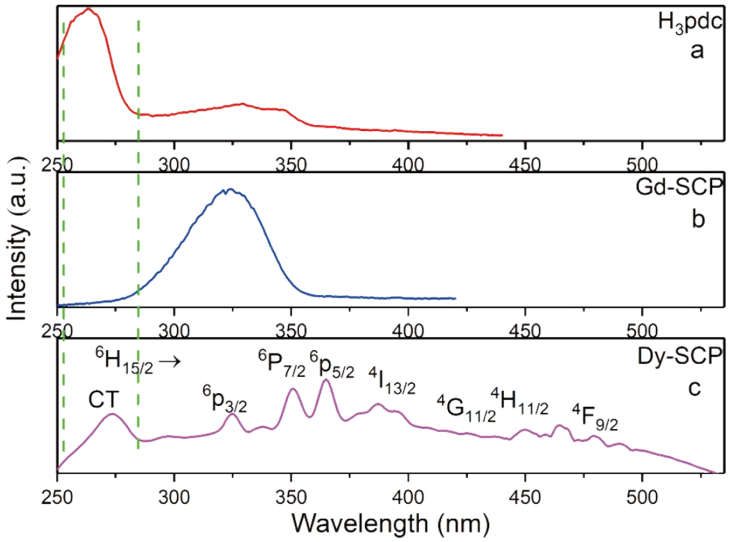

Fig. S15 Excitation spectra of (a) H_3PDC, (b) Gd-SCP and (c) Dy-SCP monitored at 460nm, 525nm and 573nm, respectively, at 298 K.

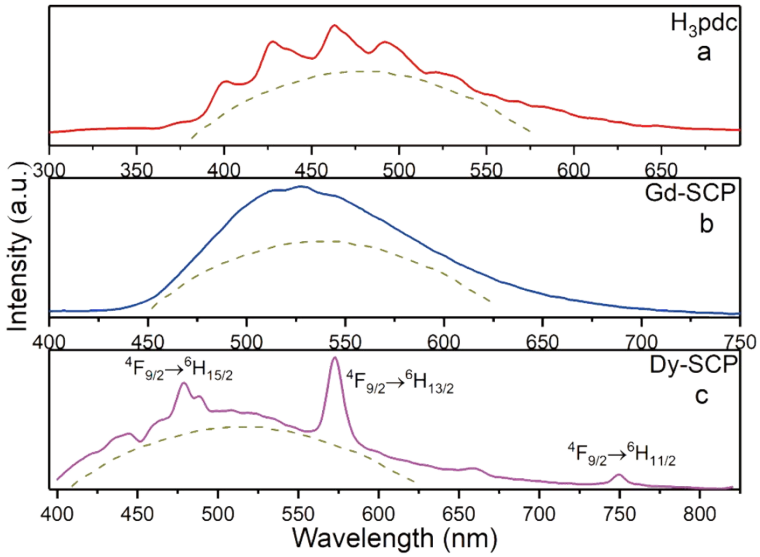

Fig. S16 Emission spectra of (a) H_3PDC, (b) Gd-SCP and (c) Dy-SCP monitored at 263nm, 323nm and 365nm, respectively, at 298 K.

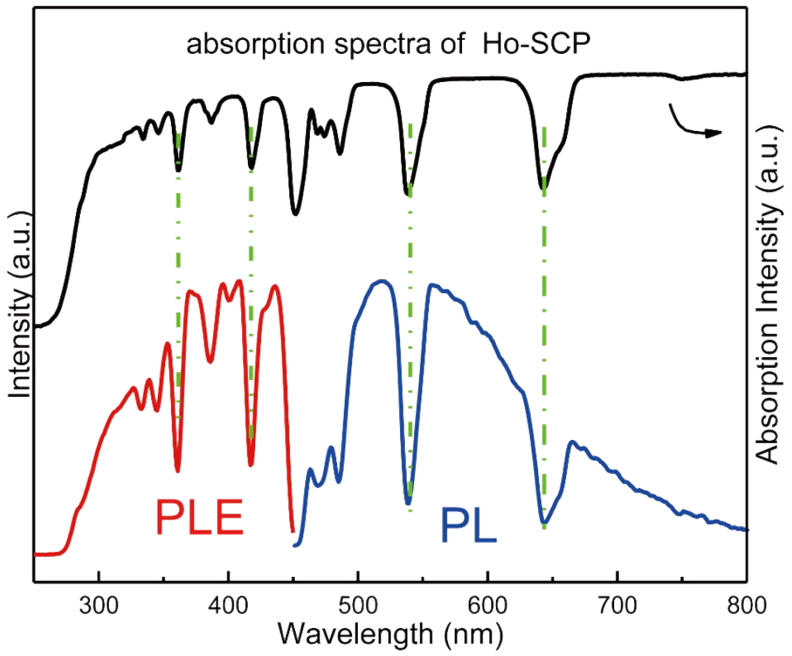

Fig. S17 Excitation spectrum of Ho-SCP monitored at 560 nm (in red) and Emission spectrum of Ho-SCP monitored at 323 nm (in blue) at 298 K, consistent with the adsorption spectrum of Ho-SCP (in black).

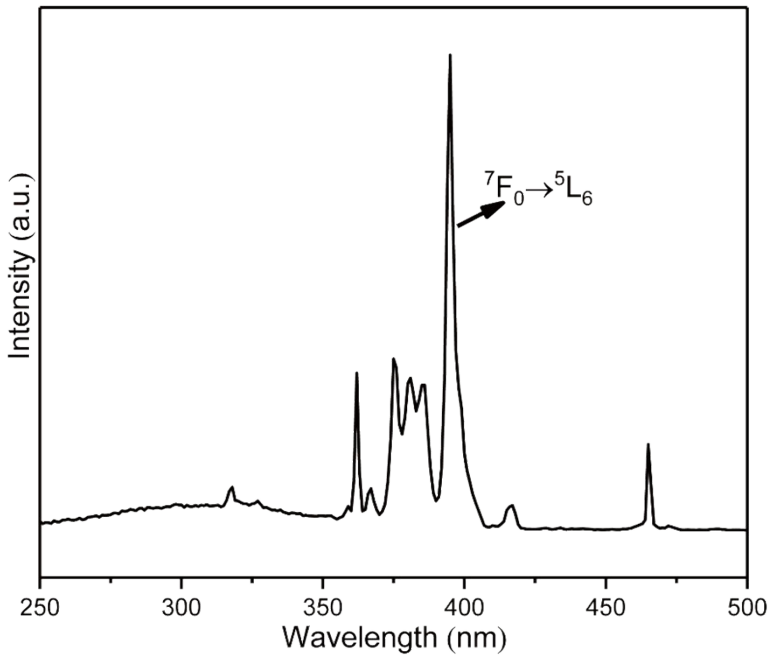

Fig. S18 Excitation spectrum of Eu-SCP at 298 K.

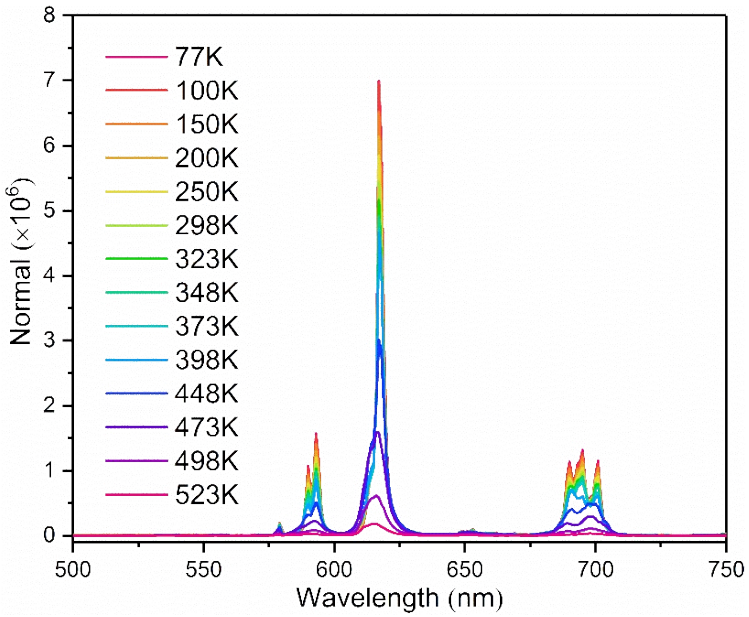

Fig. S19 Fluorescence emission spectra (λ_{ex} = 395 nm) of Eu-SCP between 77 and 523 K.

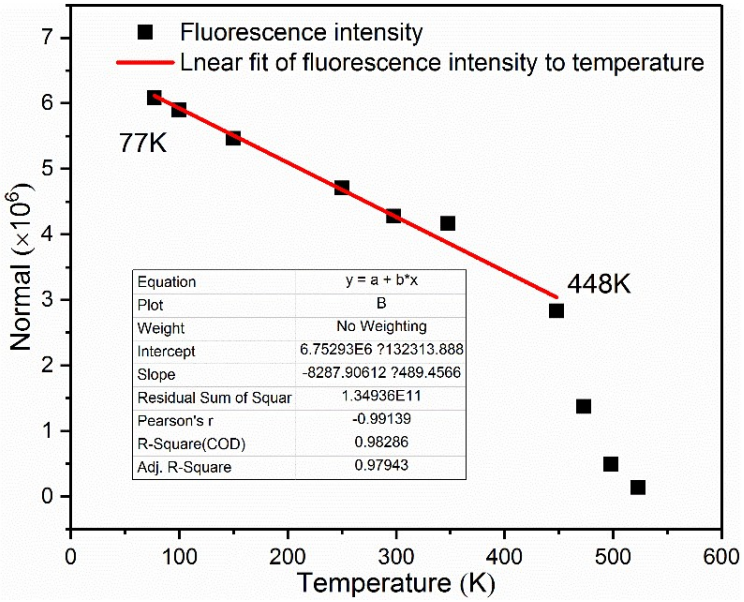

Fig. S20 Linear Fitting of fluorescence intensity to temperature of Eu-SCP. It can be seen that there is a gradual decrease in the fluorescent intensity with rising the temperature from 77 to 448 K, following a linear correlation, then a more rapid drop because of the fluorescence significantly quenched when the temperature > 448 K. This deviation from the linear fitting at temperature > 448 K is probably owing to the departure of the bonded water molecules.

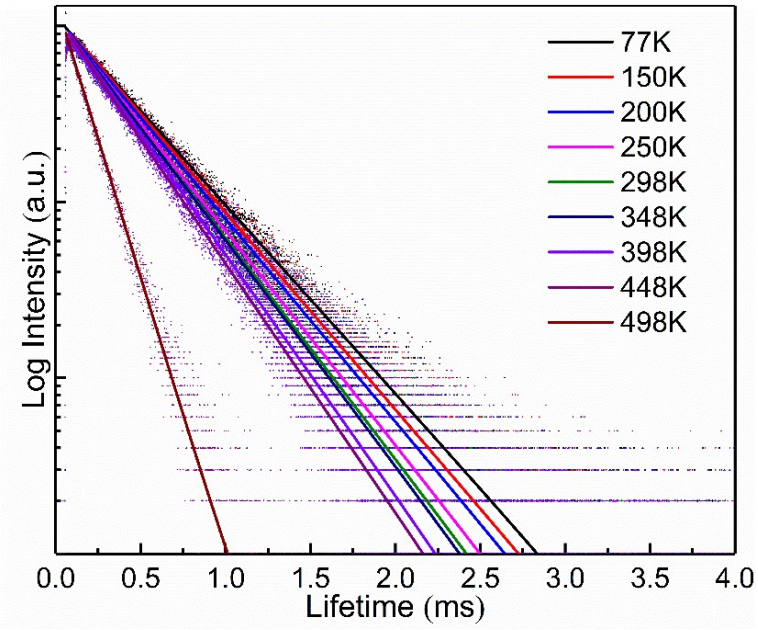

Figure. S21 Temperature-dependent fluorescence lifetime diagram of Eu-SCP (77 ~ 498 K). It can be seen that the fluorescence lifetime of Eu-SCP decreases with increasing temperature, also obeying the linear relationship in the temperature range < 448 K.

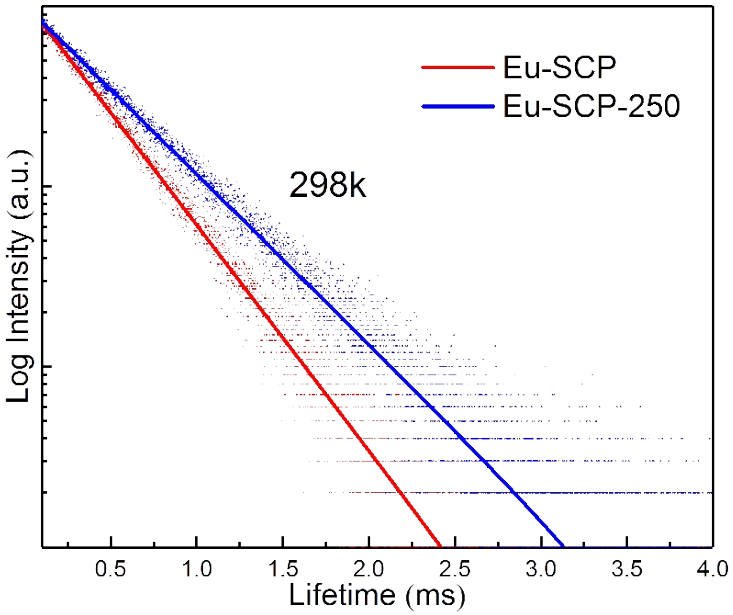

Figure. S22 Fluorescence emission decays of fresh Eu-SCP and dehydrated Eu-SCP heated at 250 °C (λ_{ex} = 395 nm, λ_{em} = 395 nm, lifetime = 348 μs for fresh Eu-SCP, 462 μs for dehydrated Eu-SCP) at 298 K.

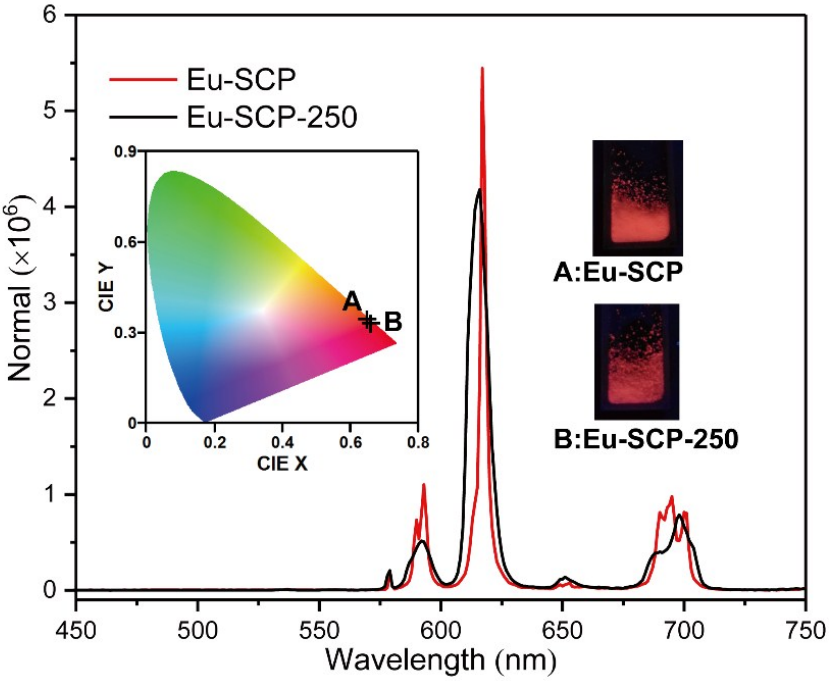

Figure. S23 Fluorescence emission spectra of A: Eu-SCP (with CIE of x = 0.6481, y = 0.345) and B: Eu-SCP-250 (activated at 250 °C, with CIE x = 0.6632, y = 0.3348) at 298 K. By comparison, the dehydrated Eu-SCP displayed slightly wider fluorescence emission peak and longer fluorescence lifetime than the freshly-synthesized sample.

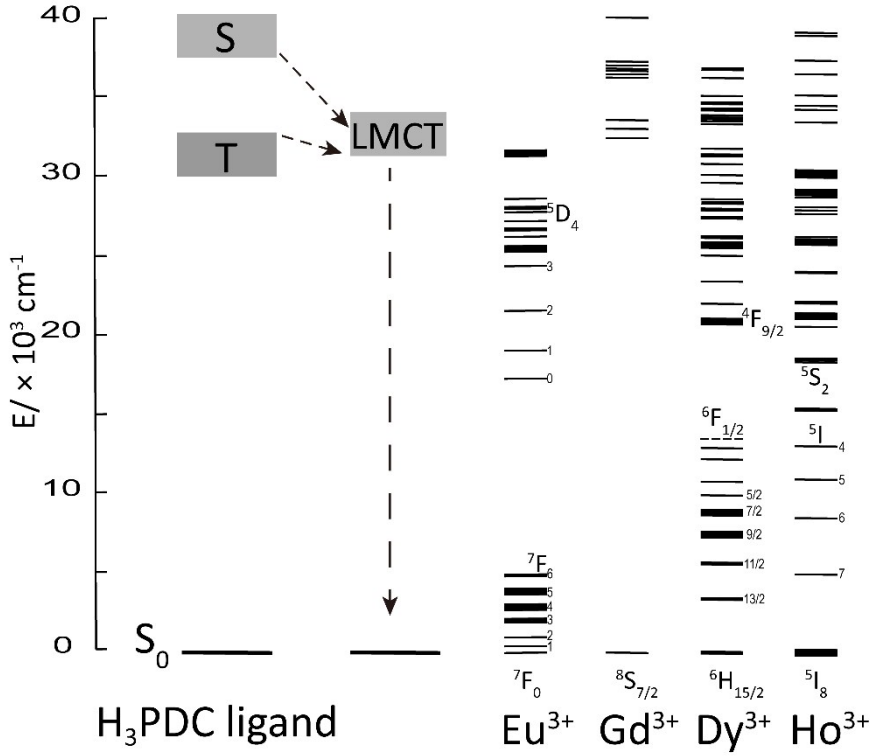

Figure. S24 Energy level diagram of Eu^{3+}, Gd^{3+}, Dy^{3+} and Ho^{3+} ions and H_3PDC ligand,

referring to the related literature on LMCT energy transfer.[1] The dashed arrows represent possible non-radiative energy transfer pathways.

All the compounds were monitored at the positions of the maximum excitation/emission peaks. There is an intense adsorption band centered at 250 nm in the UV-Vis adsorption spectrum of H_3PDC (Fig. S15), which could be attributed to π-π* electron transition. The emission spectrum (Fig. S16b) of Gd-SCP has a broad band originated from the PDC^{3-} ligand, because the excited energy level of Gd^{3+} ion is much higher than the energy level of ligand triplet state, namely where ligand to metal energy transfer (LMCT) process has been inhibited. Dy-SCP not only has the characteristic peaks related to Dy^{3+} ion but also has the typical band of PDC^{3-} ligand (Fig. S15c and Fig. S16c). As shown in the Fig. S17, the downward peaks of the emission spectrum of Ho-SCP could be due to the cancellation of PDC^{3-} characteristic band by the Ho^{3+} ion. Among Ln-SCP, only Eu-SCP displays the fluorescence that can be seen by naked eyes. As shown in Fig. S14, the characteristic band of PDC^{3-} ligand is shaded by the strong emission peaks in relation to $5D^0$-$5F^n$ (n = 0,1,2,3,4) transitions of Eu^{3+} ion, which indicates the effective ligand to metal energy transfer of Eu-SCP.

Section S12: Magnetism

(a) Plots of $\chi_m T$ and χ_m^{-1} versus T

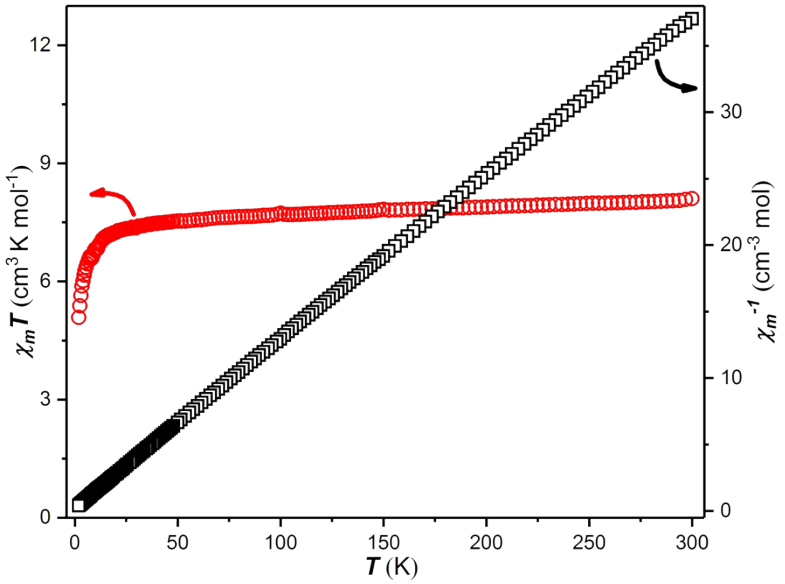

Fig. S25 Temperature dependence of $\chi_m T$ and χ_m^{-1} for Gd-SCP.

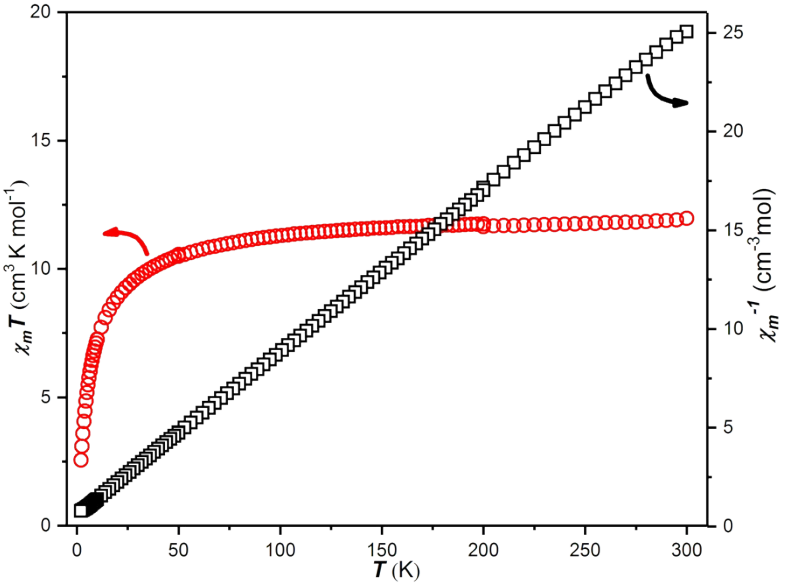

Fig. S26 Temperature dependence of $\chi_m T$ and χ_m^{-1} for Dy-SCP.

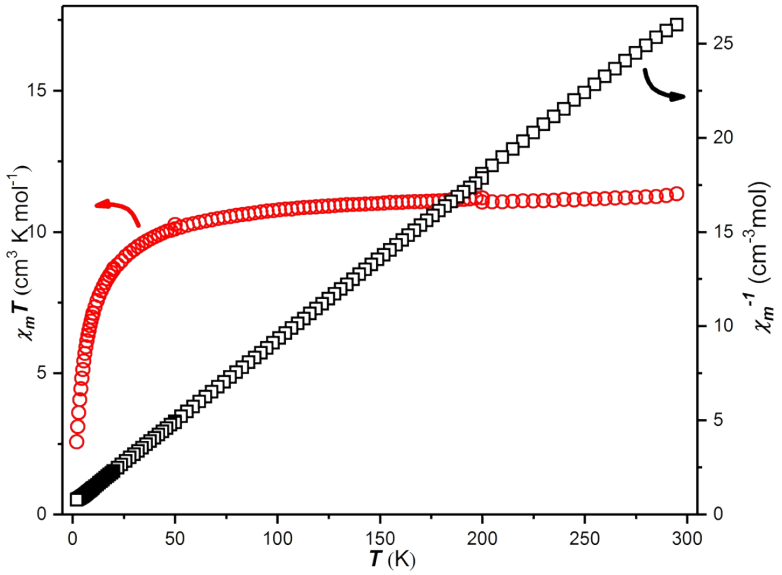

Fig. S27 Temperature dependence of $\chi_m T$ and χ_m^{-1} for Ho-SCP.

(b) Plots of χ_m' and χ_m'' versus T

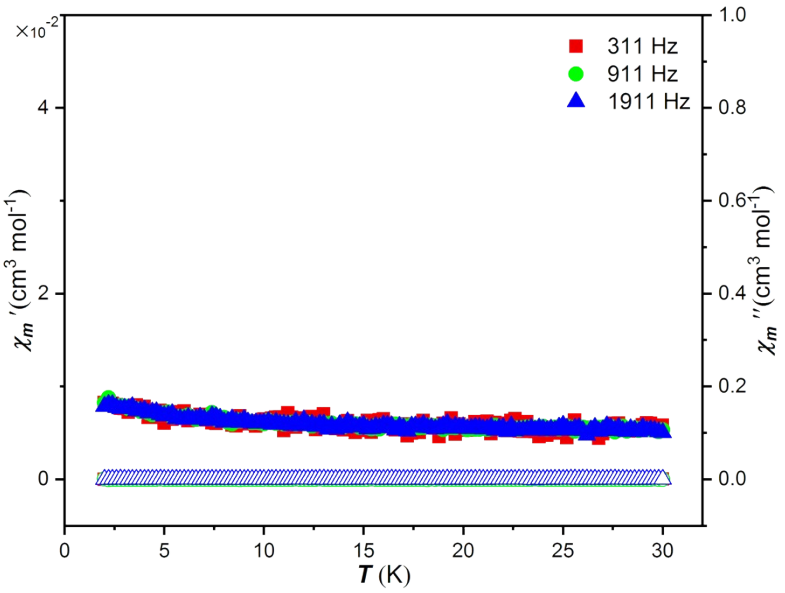

Fig. S28 Temperature dependence of ac susceptibilities, χ_m' and χ_m'', at different frequencies for Eu-SCP.

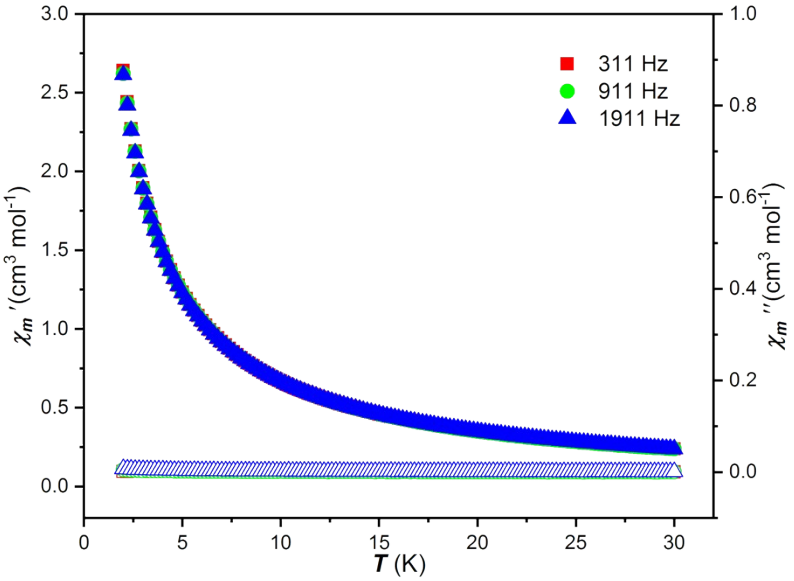

Fig. S29 Temperature dependence of ac susceptibilities, χ_m' and χ_m'', at different frequencies for Gd-SCP.

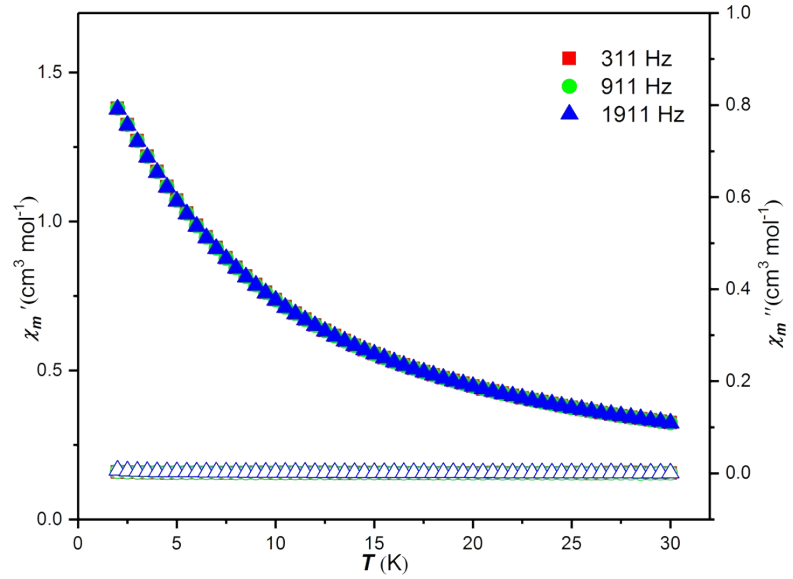

Fig. S30 Temperature dependence of ac susceptibilities, χ_m' and χ_m'', at different frequencies for Dy-SCP.

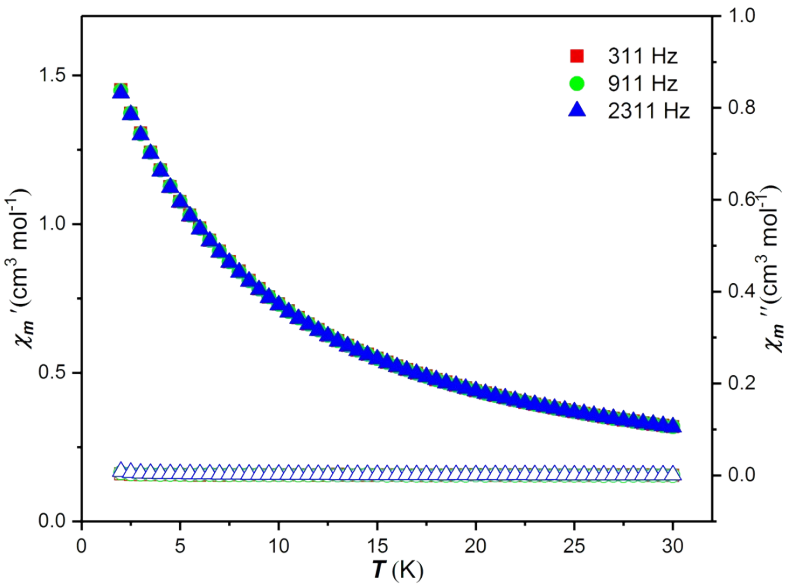

Fig. S31 Temperature dependence of ac susceptibilities, χ_m' and χ_m'', at different frequencies for Ho-SCP.

(c) Plots of *M* veusus *H*

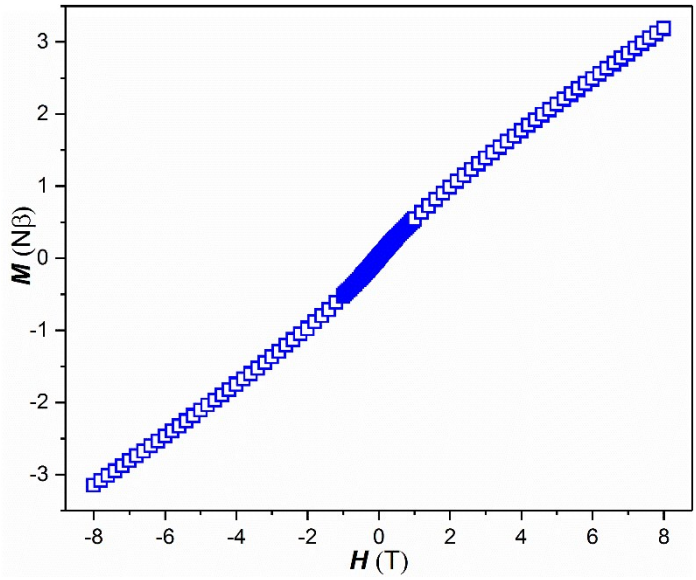

Fig. S32 Plot of *M* versus *H* for Eu-SCP.

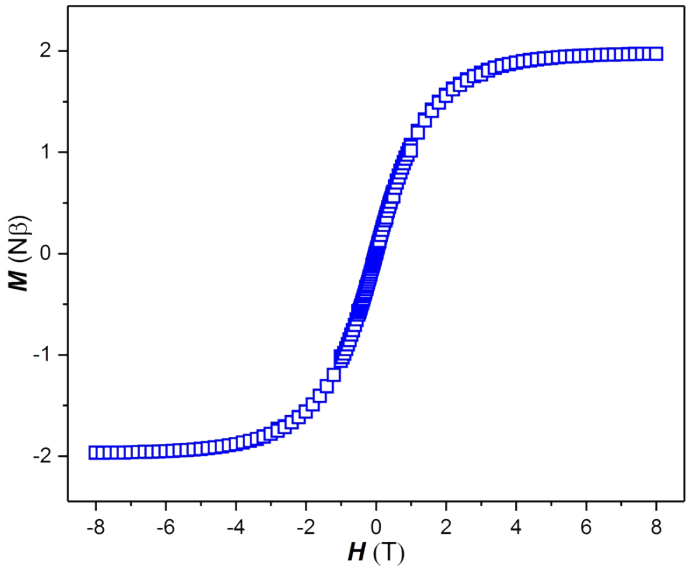

Fig. S33 Plot of *M* versus *H* for Gd-SCP.

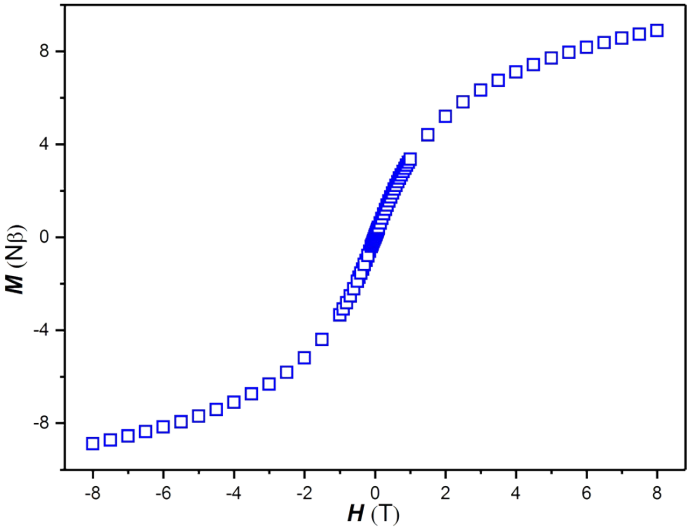

Fig. S34 Plot of *M* versus *H* for Dy-SCP.

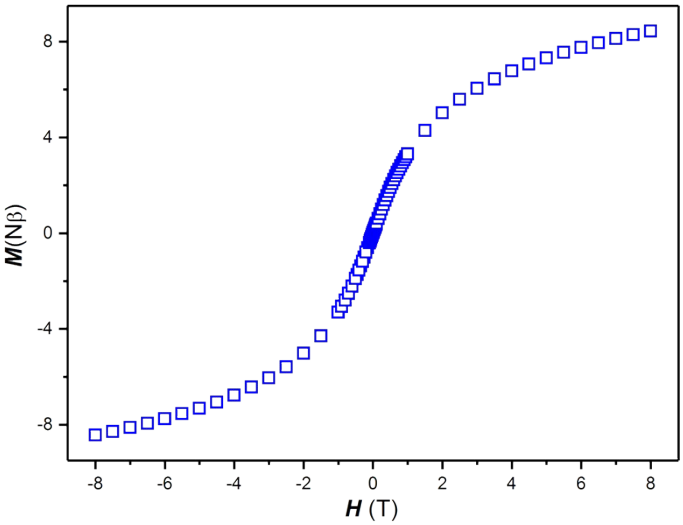

Fig. S35 Plot of *M* versus *H* for Ho-SCP.

Section S13: Proton conduction

Impedance analysis: The samples were put into a home-made mold with a radius of 0.2 cm to get circular pellets, whose thickness was measured by a Vernier caliper. Then the pellets were smeared on both sides by silver colloid, which were for fixing copper wires. The proton conductive capacities were estimated by using a Zahner (IM6) electrochemical impedance spectrometer, over a frequency range from 100 mHz to 10 MHz, under varying temperatures (25 to 65 °C) and different relative humidity (RH, 33% to 97%). The proton conductivity was calculated by using the following equation

$$\sigma = \frac{l}{SR}$$

where σ is the conductivity (S cm^{-1}). l is the thickness (cm) of the pellet, S is the cross-sectional area (cm^{-2}) of the pellet, R is the bulk resistance (Ω). The activation energy (E_a) was calculated from the following equation

$$\ln \sigma_T = \ln\sigma_0 - \frac{Ea}{KT}$$

where σ is the conductivity (S cm^{-1}), K is the Boltzmann constant (eV/K) and T is the temperature (K).

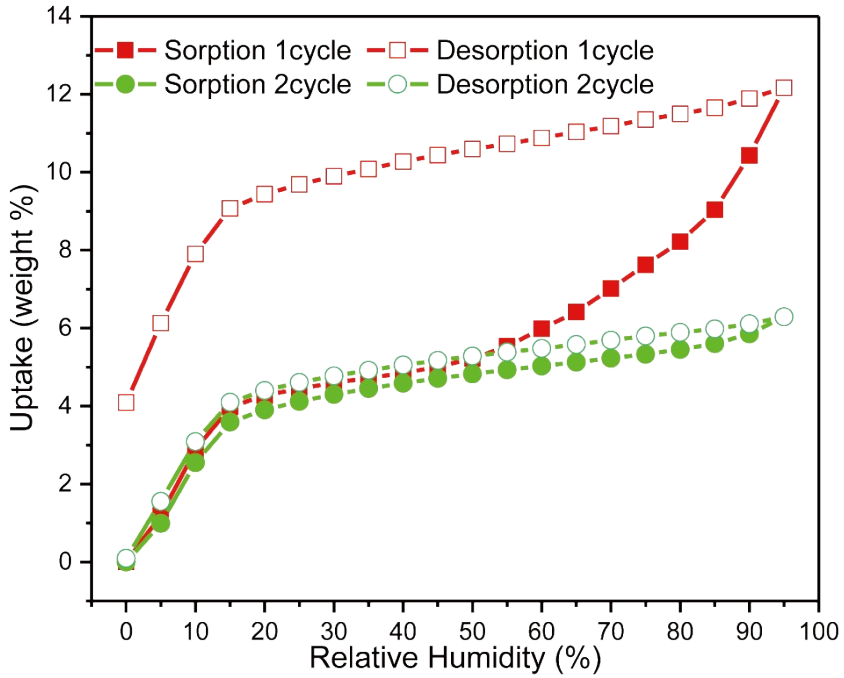

Fig. S36 Water vapor adsorption-desorption isotherms of Eu-SCP.

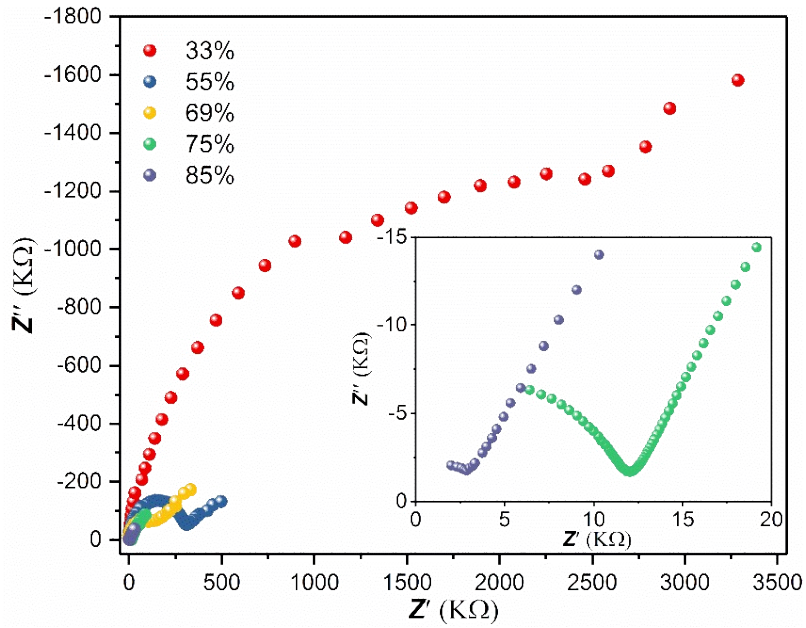

Fig. S37 Nyquist plots (at different RH) of Eu-SCP pre-heated to 190 °C.

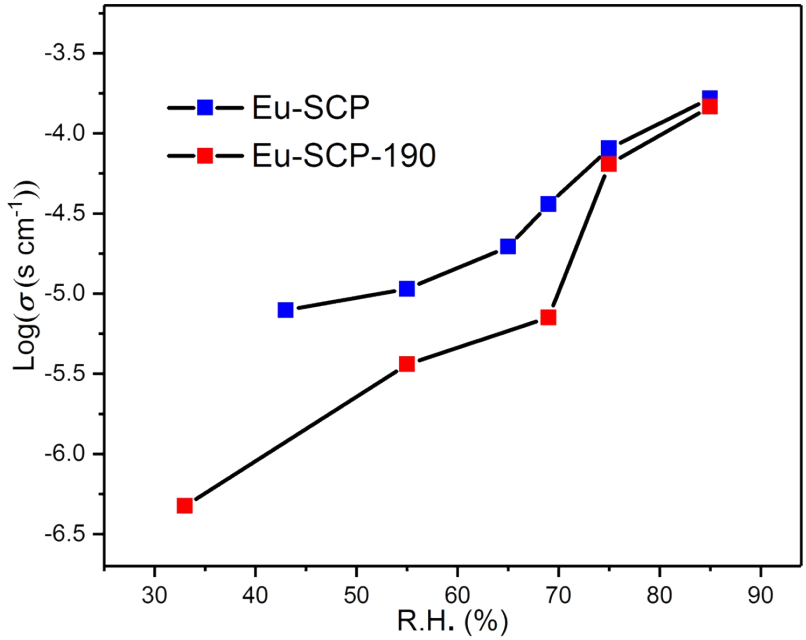

Fig. S38 Relative humidity dependences of proton conductivity of the freshly-synthesized Eu-SCP and its dehydrated form (pre-heated at 190 °C) at room temperature. Under < 75% RH, its σ values are significantly lower than that of the sample untreated thermally; while at >75% RH, two sets of σ data are close to each other. By comparing σ values of as-synthesized and thermally-treated samples, it could be concluded that the coordinated and free water molecules significantly contribute to proton conduction.

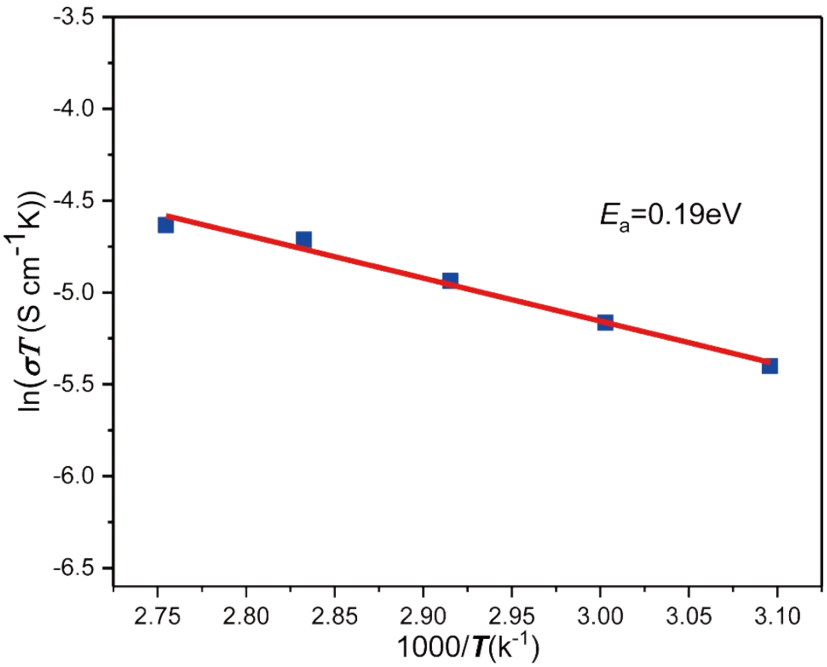

Fig. S39 Arrhenius plot of proton conductivity of Eu-SCP under 55% R.H. condition.

Table S2 List of the selected studies with high proton conductivity at 298-313 K

Compound	σ / S cm^{-1}	E_a / eV	Condition	Reference
EuL	1.0×10^{-7}	0.91	25 °C, 97% R.H.	2
DyL	1.52×10^{-7}	0.87	25 °C, 97% R.H.	2
$LaCr(ox)_3 \cdot 10H_2O$	1.0×10^{-5}	0.32	25 °C, 95% R.H.	3
$[Eu_2(CO_3)(ox)_2(H_2O)_2] \cdot 4H_2O$	1.01×10^{-5}	0.47	25 °C, 0% R.H.	4
YbO(OH)P-CEFs	7.61×10^{-5}	0.57	25 °C, 95% R.H.	5
NdTBP-CEFs	2.38×10^{-4}	0.32	25 °C, 95% R.H.	5
CoLa-II-SC	3.05×10^{-4}	0.42	25 °C, 95% R.H.	6
GdHPA-II	3.2×10^{-4}	0.23	25 °C, 95% R.H.	7
Eu-SCP	1.19×10^{-3}	0.19	21 °C, 98% R.H.	This Work
PCMOF-5	1.3×10^{-3}	0.16	25 °C, 97% R.H.	8
$N_2H_5[CeEu(C_2O_4)_4(N_2H_5)] \cdot 4H_2O$	3.42×10^{-3}	0.1	25 °C, 100% R.H.	9
$N_2H_5[Nd_2(C_2O_4)_4(N_2H_5)] \cdot 4H_2O$	2.7×10^{-3}	0.11	25 °C, 100% R.H.	9

Section S14: References

[1] C. B. Liu, R. A. S. Ferreira, F. A. Almeida Paz, A. Cadiau, L. D. Carlos, L. S. Fu, J. Rocha and F. N. Shi, *Chem. Commun.*, 2012, **48**, 7964-7966.

[2] M. Zhu, Z.-M. Hao, X.-Z. Song, X. Meng, S.-N. Zhao, S.-Y. Song and H.-J. Zhang, *Chem. Commun.*, 2014, **50**, 1912-1914.

[3] H. Ōkawa, M. Sadakiyo, K. Otsubo, K. Yoneda, T. Yamada, M. Ohba and H. Kitagawa, *Inorg. Chem.*, 2015, **54**, 8529-8535.

[4] X. Zhao, M. Wong, C. Mao, T. X. Trieu, J. Zhang, P. Feng and X. Bu, *J. Am. Chem. Soc*., 2014, **136**, 12572-12575.

[5] C. Xiao, Y. Wang, L. Chen, X. Yin, J. Shu, D. Sheng, Z. Chai, T. E. Albrecht-Schmitt and S. Wang, *Chem-Eur. J.*, 2015, **21**, 17591-17595.

[6] S.-S. Bao, K. Otsubo, J. M. Taylor, Z. Jiang, L.-M. Zheng and H. Kitagawa, *J. Am. Chem. Soc*., 2014, **136**, 9292-9295.

[7] R. M. P. Colodrero, K. E. Papathanasiou, N. Stavgianoudaki, P. Olivera-Pastor, E. R. Losilla, M. A. G. Aranda, L. Leon-Reina, J. Sanz, I. Sobrados, D. Choquesillo-Lazarte, J. M. Garcia-Ruiz, P. Atienzar, F. Rey, K. D. Demadis and A. Cabeza, *Chem. Mater.*, 2012, **24**, 3780-3792.

[8] J. M. Taylor, K. W. Dawson and G. K. H. Shimizu, *J. Am. Chem. Soc*., 2013, **135**, 1193-1196.

[9] K. Zhang, X. Xie, H. Li, J. Gao, L. Nie, Y. Pan, J. Xie, D. Tian, W. Liu, Q. Fan, H. Su, L. Huang and W. Huang, *Adv. Mater.*, 2017, **29**, 1701804.